Central European Journal of Energetic Materials
ISSN 1733-7178; e-ISSN 2353-1843

Cent. Eur. J. Energ. Mater. 2019, *16*(1): 3-20; DOI: 10.22211/cejem/104383
Article is available in PDF-format, in colour, at: http://www.wydawnictwa.ipo.waw.pl/CEJEM.html

Research paper

Assessment of Detonation Performance and Characteristics of 2,4,6-Trinitrotoluene Based Melt Cast Explosives Containing Aluminum by Laser Induced Breakdown Spectroscopy

Amir Hossein Rezaei, Mohammad Hossein Keshavarz,* Masoud Kavosh Tehrani, Mohammad Reza Darbani**

Malek-ashtar University of Technology,
83145/115 Shahin-shahr, Islamic Republic of Iran
*E-mails: *keshavarz7@gmail.com; **m.kavosh.tehrani@gmail.com*

Abstract: Aluminized melt cast formulations based on 2,4,6-trinitrotoluene (TNT) deliver an enhanced blast effect because the secondary combustion process of aluminum (Al) occurs beyond the detonation zone. A new method is introduced to assess the detonation performance and characteristics of aluminized TNT explosives on the basis of the laser-induced breakdown spectroscopy (LIBS) technique, in both air and argon (Ar) atmospheres. The plasma emissions of the prepared samples were recorded, where the atomic lines of Al, C, O and H as well as the molecular bands of AlO, CN and C_2 were identified. A good discrimination and separation between the samples was possible using LIBS and principle component analysis (PCA), although they had similar atomic compositions. The quantitative calibration curve obtained using the relative intensity of Al/O was used to determine the detonation velocity/pressure and aluminum content of the TNT/Al samples. Comparisons between experimental and theoretical spectra were made using a Nelder–Mead temperature program for CN bands, which provided good agreement with the fitted spectra. Finally, CN vibrational temperatures were calculated from these spectral fittings. These temperatures have higher values in an Ar atmosphere than in an air atmosphere. Thus, increasing the oxygen concentration can decrease these temperatures in TNT/Al standard samples.

Keywords: laser induced breakdown, spectroscopy, molecular structure, chemical analysis

1 Introduction

Energetic materials containing hazardous energetic groups, such as nitro, nitramine and nitrate functional groups, can be used as explosives, propellants and pyrotechnics [1-4]. The detonation velocity [5] and pressure [6], as well as the sensitivity to external stimuli such as impact [7], friction [8], electric spark [9], heat [10] and blast shock [11] are important properties for the assessment of explosives. Melt cast explosive compositions based on 2,4,6-trinitrotoluene (TNT) are used for a wide range of ordnance [1]. They have the availability of TNT at an economical cost and ease of processing. They exist all over the globe for a wide range of artillery shells, tank ammunitions and missile warheads [12].

Aluminum powder (Al) is widely used in explosives to enhance air blast, increase the bubble energies in underwater weapons, and create incendiary effects [13, 14]. The addition of Al creates non-ideal explosives, with long and sequential reaction zones that have been widely used in modern weapons. In contrast to ideal explosives, the assessment of the detonation performance of aluminized explosives is more complicated, and is mainly evaluated using the steel plate, cylinder and underwater tests [15, 16]. For the metal plate acceleration test and the cylinder test, the effective acting time is no more than 40 μs while aluminum powder needs hundreds of microseconds to react completely after an explosive detonation [17]. Aluminized explosives deliver an enhanced blast effect because of the secondary combustion of Al. This process beyond the detonation zone is extensively used in blast ammunition/warheads. The detonation products generated at high temperatures can react with Al, and produces energy due to these exothermic reactions. Thus, Al increases the duration of the explosive detonation pressure. Meanwhile, the delivered detonation pressure of aluminized explosives is reduced compared to the corresponding non-aluminized compositions due to the inert nature of Al [18]. The addition of large Al mass fractions to TNT can improve the spatial mixing of hot fuels with the oxidizing gases in the detonation products and chamber air, and result in a more efficient afterburning energy release [19]. Tritonal contains 80% TNT and 20% flaked Al, and was developed in USA during World War II for realizing improved blast ammunition. It can be used for fragmentation and air-blast applications, particularly in navy and air force bombs [18]. For Tritonal, it was found that approximately 66% of the Al was reacting with the detonation products in a TNT/Al composition [20].

For the composition TNT/RDX/Al, where RDX is cyclotrimethylene-trinitramine, increasing the Al/O ratio initially enhances the shock wave energy

in water. The shock energy reaches a maximum when the Al/O ratio is equal to 0.4, and then gradually decreases, whereas the bubble energy continuously increases [21]. As the Al/O ratio fluctuates between 0.3 and 0.4 in RDX/Al, *i.e.* Al content varies between 20% and 30%, the shock wave energy reaches a maximum value. On further increasing the Al content, the shock wave energy drops but the bubble energy increases continuously [22]. The shock wave energy and the bubble energy can also be changed by the Al content in cyclotetramethylenetetranitramine/Al (HMX/Al) compositions. The detonation pressure and velocity decrease with increasing Al percentage in HMX/Al. The detonation heat has a tendency to initially increase followed by a parabolic decrease with increasing Al/O ratios. When the Al content equals 20-30%, the shock wave energy and the bubble energy exhibit maximum values [23]. For underwater explosives, it was found that the energy output structure is not only related to the Al/O ratio, but also to the size of the Al particles, the oxidation capacity of the explosive, and chemical thermodynamics [24, 25]. Addition of nanometric Al to the TNT/Al system leads to a remarkable increase in velocity of detonation as well as heat of detonation [26].

Laser-induced breakdown spectroscopy (LIBS) can determine the elemental composition on the basis of elemental and molecular emission intensities. Since LIBS has certain advantages, such as no sample preparation, high sensitivity, and real-time detection, it has been widely used for numerous applications. Some attempts have been made to use LIBS for the detection of explosives [13, 27-30]. Selected diatomic molecular emissions were also used to study the spectroscopic signatures of molecular compounds [31]. Molecular emissions can yield a deeper understanding of the principal formation routes of molecular species existing in laser-induced plasmas [32]. Molecular components may be formed from ablated material. Thus, the excited atoms may recombine with ions or with air components in the laser-induced plasma. For aluminized energetic compounds, three molecular species, AlO, CN and C_2, are observed in like manner [13, 33, 34].

Spectral analysis can either generate qualitative information or be used to calculate concentrations [35]. Principle component analysis (PCA), and partial least squares discriminant analysis (PLS-DA) have been used for the identification of organic compounds by the LIBS method [36]. PCA can discriminate between two classes of spectra and outliers. It can visualize similarities between spectra by graphically representing them in a new space with much fewer dimensions, which retain most of the information contained in the data set [37, 38].

For quantitative analysis, the calibration curve method is one of the most popular methods in which a curve is drawn between the integrated intensity

of the atomic emission of the element and the corresponding concentration of that element in standard samples. The calibration curve can determine the concentration of an element in an unknown sample by measuring the intensity of the corresponding atomic emission in the LIBS spectra of the sample. This is most practical because the standard or certified reference material (CRM) is easily available [39-41].

The purpose of the present work was to use the LIBS technique for an assessment of the performance of TNT-based aluminized explosives. At first, PCA methods were used to identify and classify the aluminized TNT samples. Since the detonation performance of an aluminized explosive is related to the Al content of the explosive [42-45], this work can determine both the detonation performance and the Al content. Air and argon (Ar) atmospheres were used to investigate the aluminized TNT samples. It was shown that the formation mechanism of the AlO, CN and C_2 molecular bands is related to the Al percentage in the aluminized TNT composition, as well as the oxygen content in the plasma. Moreover, the quantitative calibration curve obtained using the relative intensity of Al/O was used to determine the detonation velocity/pressure and the Al content of TNT/Al samples.

2 Materials and Methods

2.1 LIBS setup

LIBS tests were performed using a LIBSCAN 100 apparatus (Applied Photonic LTD, United Kingdom), which consists of different components. The laser source was a Q-switched Nd:YAG with 1064 nm wavelength and 7 ns pulse duration. The laser pulse energy varied from 10 mJ to 100 mJ, where the maximum laser irradiance for a beam focused on the sample was up to 1.4 GW/cm^2. The plasma emissions were transferred to the detector unit by an optical system and optical fiber bundle. Eight spectrometers (Avantes-20-01-13-A, Netherland), with 0.04 nm resolution for spectral analysis from 182 nm to 1057 nm coupled with CCD, were used for recording the spectra. The delay time between the laser and spectral recording and integration window (gate time) was adjustable. The minimum delay and gate times were 1.27 μs and 1.1 ms, respectively. In an ablation chamber, the sample was inserted on a X, Y, Z translation stage that was controlled by internal software. The final spectra were obtained by averaging twenty spectra from each sample.

2.2 Materials

Table 1 shows four types of TNT-based aluminized explosives, which were prepared as standard samples. These samples had different weight percentages of TNT (<800 μm particle diameter) and Al powder (typically ~50 μm average diameter), and were prepared by compressing the powders using a standard press. The pellet's diameter and thickness were estimated to be 13 mm and 3-4 mm, respectively. The LIBS measurements were performed in both air and Ar atmospheres. The Ar flow at ~5 L⁄min was directed across the sample surface. This atmosphere reduced the atmospheric recombination of nitrogen and oxygen atoms.

Table 1. Weight percentages and chemical formulas of TNT-based aluminized explosives

Standard sample	Content [%]		Formula
	TNT	Al	
1	95	5	$C_{2.929}H_{2.092}N_{1.255}O_{2.511}Al_{0.185}$
2	90	10	$C_{2.775}H_{1.982}N_{1.189}O_{2.378}Al_{0.370}$
3	85	15	$C_{2.621}H_{1.872}N_{1.123}O_{2.246}Al_{0.555}$
4	80	20	$C_{2.467}H_{1.762}N_{1.057}O_{2.114}Al_{0.741}$

3 Results and Discussion

3.1 Spectral line identification

The LIBS spectrum of the standard sample of TNT/Al (80/20) is shown in Figure 1. Each wavelength of the peaks in the spectrum was analyzed thoroughly, compared, and finally identified with the help of the US National Institute of Standards and Technology database [46]. Figures 1(a) and 1(b) show the LIBS spectra obtained from the TNT/Al (80/20) standard sample in: (a) air atmosphere with the wavelength range 230-800 nm, and (b) Ar atmosphere with wavelength range 245-850 nm. The spectral peaks corresponding to a particular atom/molecular species are summarized in the graphs. Major elemental peaks corresponding to Al, 394.40 nm and 396.15 nm, were observed in both Figures 1(a) and 1(b). Figure 1(b) contains further peaks: C247.82 nm, H656.2 nm, O777.2 nm and Ar: 750.38 nm, 763.51 nm, 794.81 nm, 800.61 nm, 801.47 nm, 810.36 nm, and 811.53 nm lines. Peaks of some impurities, such as lithium, sodium, potassium and calcium, were also observed.

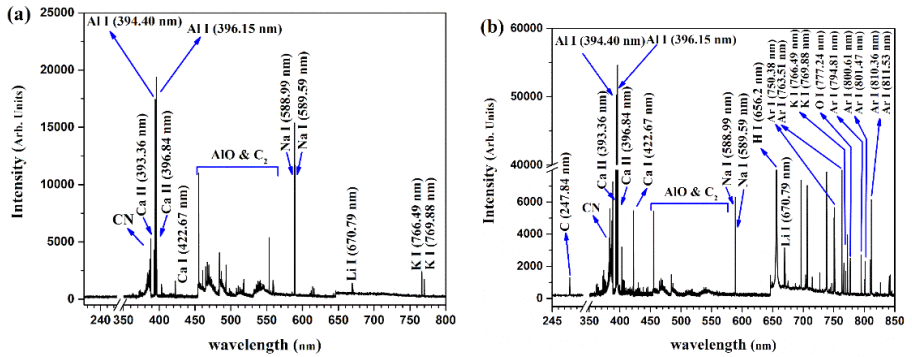

Figure 1. LIBS spectrum of the TNT/Al (80/20) standard sample in two atmospheres: (a) air; (b) Ar

Furthermore, the molecular emissions from CN, C_2 and AlO in the TNT/Al (80/20) standard sample were also observed. The CN violet band lines, corresponding to $B^2\sum^+ - X^2\sum^+$ states with transitions $\Delta v = 0$, were observed in the 388.28 nm (0–0), 387.07 nm (1–1), 386.16 nm (2–2), 385.40 nm (3–3), and 385.01 nm (4–4) regions. The spectral peaks of the C_2 Swan band system in the regions of 467-474 nm ($\Delta v = 1$), 509-517 nm ($\Delta v = 0$), and 550-564 nm ($\Delta v = -1$), and the AlO emission lines, corresponding to the $B^2\sum^+ - X^2\sum^+$ states with transitions $\Delta v = +2$ to $\Delta v = -2$, were also observed in the 450-560 nm region. These peaks have also been observed for the other samples, but there are some differences between each spectrum that correspond to composition and atmosphere.

3.2 LIBS results for the different Al content samples

Reactions (1) and (2) show the formation of AlO molecules by two different paths, which provide a greater AlO molecular emission intensity in the air atmosphere than in the Ar atmosphere.

$$Al + O_2 \rightarrow AlO + O \quad (1)$$

$$Al + O + M \rightarrow AlO + M \quad (2)$$

Figure 2(a) displays the bar diagrams of the AlO intensities, at the 464.83 nm wavelength *versus* Al content for the TNT/Al standard samples, in the two atmospheres. As seen, the emission intensities of AlO are increased in the air atmosphere compared to the Ar atmosphere, due to depletion of Al emissions according to reactions (1) and (2) [13, 14].

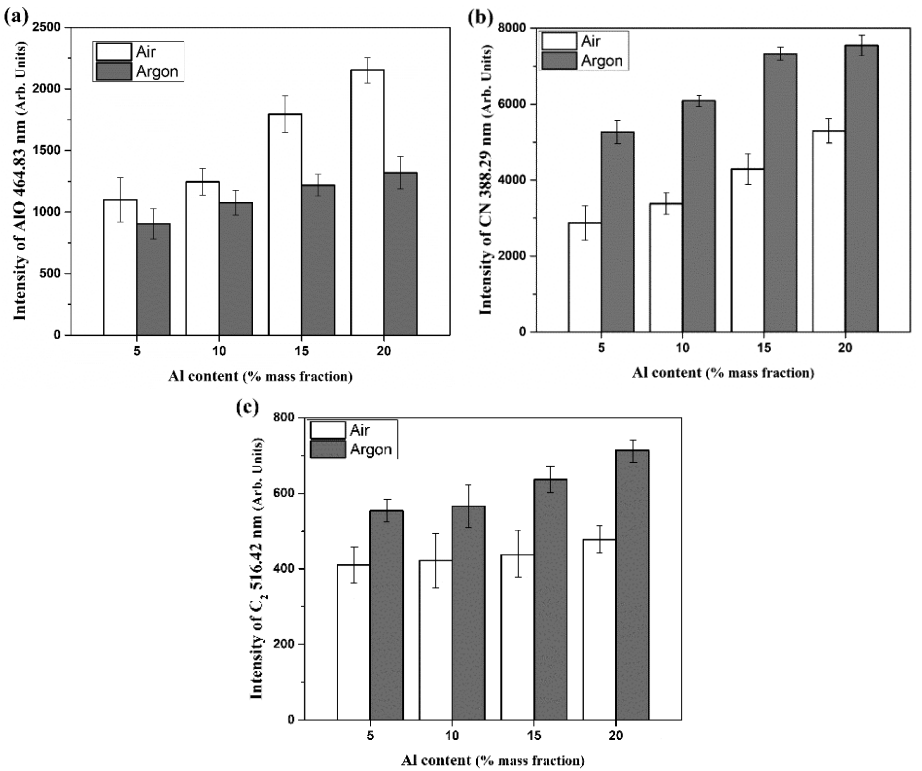

Figure 2. Bar diagrams of (a) AlO (464.83 nm), (b) CN (388.29 nm), (c) C_2 (516.42 nm); intensities versus Al content in TNT/Al standard samples for comparison intensities, in two atmospheres (air and Ar)

The origin and routes of molecule formation can be cited by: (a) fragmentation of the original compound to form carbon dimers and CN molecules; (b) production of CN; and (c) formation of both C_2 and CN [34]. Reactions (3)-(5) refer to the formation of CN molecules. For the air atmosphere, CN is formed by recombination of C with atmospheric nitrogen, while the formation of CN results from the carbon and nitrogen of the molecule in the Ar atmosphere [47].

$$2C + N_2 \rightarrow 2CN \quad (3)$$
$$C + N_2 \rightarrow CN + N \quad (4)$$
$$C + N + M \rightarrow CN + M \quad (5)$$

The C_2 molecular radiations of the Swan system were observed, and can be related to the aromatic ring and double-bonded carbon (C=C)

in the molecular structure of TNT [48]. Reactions (6)-(8) show important processes in forming C_2 [49].

$$2C + M \rightarrow C_2 + M \quad (6)$$
$$CN + C \rightarrow C_2 + N \quad (7)$$
$$C + CH \rightarrow C_2 + H \quad (8)$$

As seen in Figures 2(b) and 2(c), the emission intensities of the CN and C_2 bands increased as the Al content was increased from 5% to 20% in the air and Ar atmospheres, respectively, because more oxygen atoms were scavenged by Al to form AlO when the concentration of O atoms in the laser-induced plasma was decreased. For reaction (9), smaller amounts of O atoms are available in the plasma [33], which can increase the concentration of CN molecules.

$$CN + O \rightarrow CO + N \quad (9)$$

Reactions (10) and (11) show two paths for decreasing C and C_2:

$$C + O + M \rightarrow CO + M \quad (10)$$
$$C_2 + O \rightarrow CO + C \quad (11)$$

Since the concentrations of CN and C_2 molecules increase by the reactions (3-5) and (6-8), respectively, the emission intensities are larger in the Ar atmosphere compared to the air atmosphere for the samples with the same concentrations. Since the Ar atmosphere has smaller conductivity and specific heat than the air atmosphere, it is hotter and more energetic and gives the highest signal intensity [48, 50].

3.3 PCA calculation (full spectra)

Since there is a little difference between the aluminized TNT spectra, the PCA method is useful for distinguishing spectra. The PCA method was used to identify and classify the aluminized RDX samples [13, 14]. Figures 3(a) and 3(b) compare the PCA calculations for 20 spectra of aluminized TNT and aluminized RDX samples in the air and Ar atmospheres, respectively. As may be seen, the distinction between the aluminized TNT and the aluminized RDX samples with different compositions is clearer in Ar, which may be due to energetic fluctuations of the plasmas and not the intrinsic nature of the samples [28].

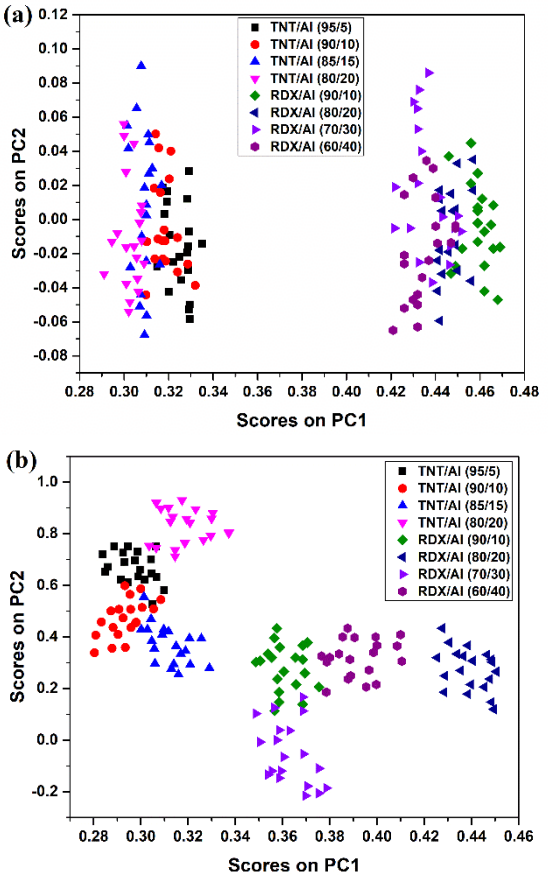

Figure 3. Two-dimensional PCA scores for aluminized TNT and aluminized RDX samples in two atmospheres: (a) air and (b) Ar

An Ar flow can be used here to displace air in order to eliminate most contributions of the oxygen and nitrogen from the air for sensitive and selective LIBS distinctions of the aluminized TNT and aluminized RDX samples. Thus, these experimental results demonstrate that there is a good discrimination and separation between the two different types of aluminized explosives.

3.4 Study of detonation performance of aluminized TNT

Detonation velocity and pressure are two important parameters for the assessment of the detonation performance of explosives. For non-ideal explosives such as aluminized TNT, in contrast to ideal explosives, reliable assessment

of the detonation properties by different computer codes is difficult [2]. They depend on different parameters, such as elemental composition, heat of formation, and the initial density [51]. For the increasing percentage of Al in the formulation of non-ideal explosives, elemental composition has an important role [52]. The measured density, the detonation parameters [53] and the Al/O composition ratio for four samples of TNT/Al are given in Table 2. The test sample charge size was 22 mm Ø × 90 mm [53].

Table 2. Composition, explosive properties and Al/O composition ratio for four TNT/Al standard samples

Standard sample	TNT [%]	Al [%]	Experimental density [g/cm^3]	Detonation velocity [km/s]	Detonation pressure [GPa]	Al/O ratio
1	95	5	1.63	6.829	19	0.07
2	90	10	1.66	6.659	18.4	0.15
3	85	15	1.68	6.528	17.9	0.25
4	80	20	1.72	6.325	17.2	0.35

As seen in Figure 4, there is a good linear relationship (regression coefficient, $R^2 > 0.99$) between the Al/O intensity ratio and the Al/O composition ratio in the TNT/Al standard samples under an Ar atmosphere. Since reliable prediction of the detonation performance of non-ideal aluminized explosives is of the utmost importance [51, 54], it is found here that there are good correlations between detonation performance and LIBS output. The relative intensities of the Al/O from LIBS measurements can be correlated with the detonation velocity and pressure of the TNT/Al standard samples.

As indicated in both Figures 5 and 6, there is a good linear correlation between the Al/O intensity ratio and detonation velocity/pressure in the TNT/Al standard samples (regression coefficient, $R^2 > 0.99$). Thus, it is possible to determine the detonation velocity and pressure of an unknown sample with a calibration curve.

3.5 Determination of the Al content in aluminized TNT

Calibration curves for the quantitative analysis of Al in Tritonal (TNT/Al:80/20) samples were prepared by measuring the integrated areas of specific atomic lines present in the LIBS spectra of the TNT/Al standard samples. The average spectra of 20 laser shots were obtained for the surface of each standard sample, which contained a specific Al content over the 5-20% range, in an Ar ambient atmosphere. As shown in Figure 7, the ratio calibration curve was drawn between

the Al content in the TNT/Al standard samples and the Al/O intensity ratio for an Ar ambient atmosphere. These data were linearly fitted, and showed a good linear relationship (regression coefficient, $R^2 = 0.9916$) with a relatively low value of the standard deviation between the Al/O intensity ratio and Al content. Thus, the Al content can be determined in TNT/Al compositions by using a calibration curve.

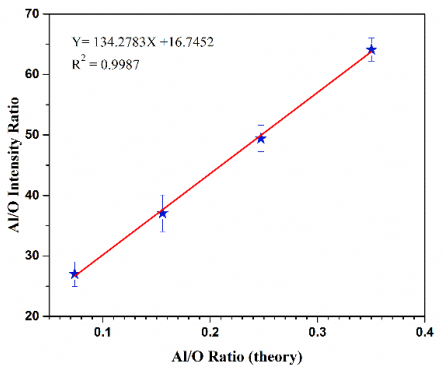

Figure 4. The measured Al/O intensity ratio by LIBS in an Ar atmosphere versus the Al/O composition ratio of TNT/Al given in Table 2

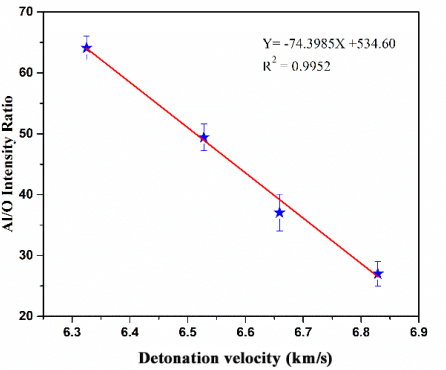

Figure 5. Al/O intensity ratio versus detonation velocity in the TNT/Al standard samples

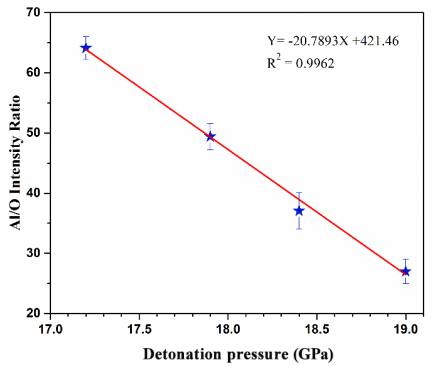

Figure 6. Al/O intensity ratio versus detonation pressure in the TNT/Al standard samples

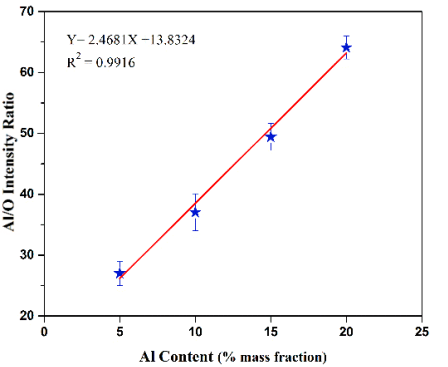

Figure 7. Calibration curve using Al/O intensity ratio versus Al content of the TNT/Al standard samples in an Ar atmosphere

In order to reduce the standard deviation and the influence of experimental parameters such as laser power, sample-to-lens distance, and the nature of the matrix elements of different samples, the intensity ratio of two atomic lines (Al/O) rather than the Al line intensity (Figures 5 to 8) has been used. It should be mentioned that the calibration curves are valid only for TNT/Al mixtures in the same %Al range (5-20%). For different particle sizes and the addition of binders or other constituents, different calibration curves are needed because they give different plasma chemistries.

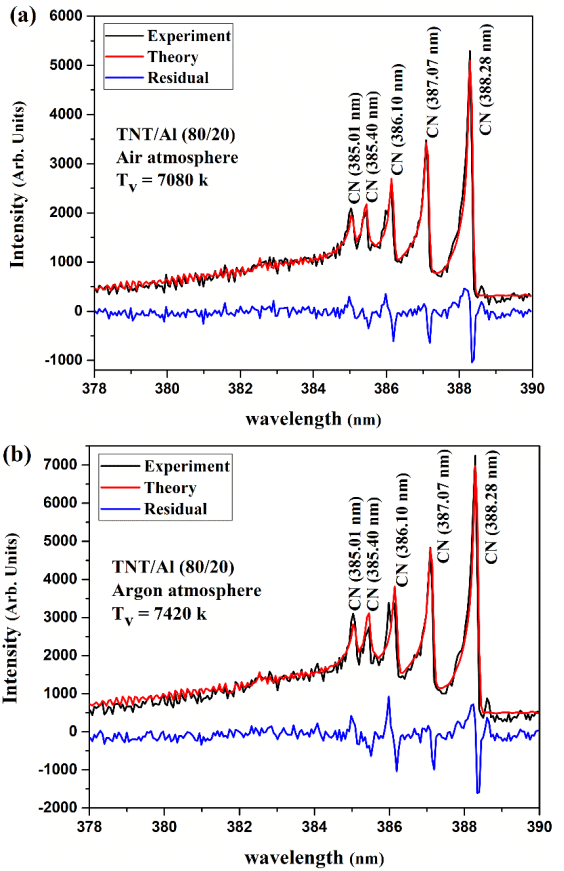

Figure 8. Comparisons between experimental and theoretical spectra, which were obtained using a NMT program for CN violet from LIB spectra of TNT/Al (80/20) standard sample of the sequence $\Delta v = 0$, in two atmospheres (a) air (b) Ar

3.6 Comparison between experimental and theoretical spectra, as well as determination of vibrational temperatures

For the CN violet band systems, a least-square fitting program NMT applying the Nelder–Mead algorithm, developed at the University of Tennessee Space Institute, was used to determined the vibrational temperatures. This program is used to produce theoretical spectra for selected diatomic molecular transitions and wavelength regions. It uses accurate line strength (Hönl-London) factors along with temperature and full-width half maximum (FWHM) values as inputs [55, 56]. Figure 9 compares the experimental data and theoretical spectra that were obtained using a NMT program for CN violet from LIB spectra of the TNT/Al (80/20) standard sample in air and Ar atmospheres of the sequence $\Delta v = 0$, respectively. As seen in both parts of Figure 9, there are clear vibrational peaks and underlying rotational structure. Experimental data showed good agreement with the fitted spectra, which provided good matching for both the vibrational and rotational parts of the spectra. Thus, local thermodynamic equilibrium (LTE) can be inferred for those cases that LTE allows, *i.e.* $T = T_{vib} = T_{rot}$ [48, 55, 56].

The vibrational temperature values, which were calculated from the spectral fitting to the CN violet band systems from the laser-produced plasmas of the TNT/Al standard samples in air and Ar atmospheres, are listed in Table 3. The program runs three times in succession to ensure accuracy of the computed temperature. The error in the vibrational temperatures reported here was about ±100 K. The standard deviations of the relative intensity of the fit in most cases were below 0.2.

Table 3. Vibrational temperatures, calculated from the spectral fitting to the CN violet band systems with the $\Delta v = 0$ sequences from laser-produced plasmas of TNT/Al standard samples in air and Ar atmospheres

Standard sample	TNT [%]	Al [%]	CN T_{vib} [K]	
			Air atmosphere	Ar atmosphere
1	95	5	6490	6870
2	90	10	6650	7020
3	85	15	6910	7290
4	80	20	7080	7420

As reported in Table 3, the CN vibrational temperatures are higher in an Ar atmosphere than in an air atmosphere for the TNT/Al standard samples of the same composition. Higher amounts of oxygen atoms are available in the plasma for an air atmosphere as compared to an Ar atmosphere,

which may provide a signal intensity of CN considerably lower because of the consumption of the CN molecular species and the formation of CO molecules. In addition, an Ar atmosphere has lower thermal conductivity and specific heat compared to an air atmosphere. Therefore, an Ar plasma is hotter and more energetic, giving the highest signal intensity [13, 14]. Furthermore, the CN vibrational temperatures are increased as the Al content in the TNT/Al standard samples is increased. Thus, the emission intensity of the CN band increases with increasing Al content from 5% to 20%, and the amount of oxygen atoms in the TNT/Al standard samples is naturally decreased.

4 Conclusions

In this work, plasma emissions of aluminized TNT/Al samples were recorded using the LIBS technique in both air and Ar atmospheres. The atomic lines of Al, C, O and H as well as the molecular bands of AlO, CN and C_2 were identified. The formation mechanisms of AlO, CN and C_2 molecular bands were related to the influence of the Al content in the compositions as well as the oxygen content present in the plasma. A smaller amount of oxygen is available in an Ar plasma to react with Al, CN and C_2, accompanied by lower conductivity and specific heat of Ar compared to an air atmosphere. Thus, the emission intensity of Al, CN and C_2 were more intense in an Ar atmosphere. The experimental results demonstrated that a good distinction is possible between aluminized TNT and aluminized RDX samples using LIBS and PCA methods. For a sensitive and selective LIBS distinction between aluminized TNT and RDX samples, an Ar flow can be used to displace air. The capability of the LIBS technique for determining the detonation parameters of TNT/Al samples was demonstrated through an investigation of the dependence of the relative intensity of the Al/O ratio to the detonation velocity and pressure. Detonation pressures and velocities decreased with increasing Al/O intensity ratio, indicating a good linear relationship ($R^2 > 0.99$). The quantitative results obtained for the calibration curve using the relative intensity of the Al/O ratio ($R^2 = 0.9916$) was used to determine the Al content of aluminized TNT. Comparisons between the experimental and theoretical spectra were made using a NMT program for CN violet bands of the sequence $\Delta v = 0$. Thus, good agreement was observed with the fitted spectra as they nearly overlap. Finally, CN vibrational temperatures were calculated from these spectral fittings. These temperatures have higher values in an Ar atmosphere than in an air atmosphere, which can decrease the temperature in the TNT/Al standard samples by increasing the oxygen concentration.

Acknowledgments

We would like to thank the research committee of Malek-ashtar University of Technology (MUT) for supporting this work. We also thank Dr. James O. Hornkohl from University of Tennessee Space Institute for providing us with the NMT code.

References

[1] Agrawal, J.P. *High Energy Materials: Propellants, Explosives and Pyrotechnics*. John Wiley and Sons, **2010**.
[2] Keshavarz, M.H.; Klapötke, T.M. *Energetic Compounds: Methods for Prediction of Their Performance*. Walter de Gruyter GmbH, **2017**.
[3] Klapötke, T.M. *Chemistry of High-energy Materials*. Walter de Gruyter GmbH and Co KG, **2015**.
[4] Keshavarz, M.H.; Klapötke, T.M.; Klapotke, T.M. *The Properties of Energetic Materials: Sensitivity, Physical and Thermodynamic Properties*. Walter de Gruyter GmbH and Co KG, **2017**.
[5] Keshavarz, M.H.; Kamalvand, M.; Jafari, M.; Zamani, A. An Improved Simple Method for the Calculation of the Detonation Performance of CHNOFCl, Aluminized and Ammonium Nitrate Explosives. *Cent. Eur. J. Energ. Mater.* **2016**, *13*(2): 381-396.
[6] Jafari, M.; Keshavarz, M.H. A Simple Method for Calculating the Detonation Pressure of Ideal and Non-Ideal Explosives Containing Aluminum and Ammonium Nitrate. *Cent. Eur. J. Energ. Mater.* **2017**, *14*(4): 966-983.
[7] Keshavarz, M.H. A New General Correlation for Predicting Impact Sensitivity of Energetic Compounds. *Propellants Explos. Pyrotech.* **2013**, *38*(6): 754-760.
[8] Keshavarz, M.H.; Hayati, M.; Ghariban-Lavasani, S.; Zohari, N. A New Method for Predicting the Friction Sensitivity of Nitramines. *Cent. Eur. J. Energ. Mater.* **2015**, *12*(2): 215-227.
[9] Keshavarz, M.H.; Pouretedal, H.R.; Semnani, A. Reliable Prediction of Electric Spark Sensitivity of Nitramines: A General Correlation with Detonation Pressure. *J. Hazard. Mater.* **2009**, *167*(1): 461-466.
[10] Keshavarz, M.H.; Moradi, S.; Saatluo, B.E.; Rahimi, H.; Madram, A.R. A Simple Accurate Model for Prediction of Deflagration Temperature of Energetic Compounds. *J. Therm. Anal. Calorim.* **2013**, *112*(3): 1453-1463.
[11] Keshavarz, M.H.; Motamedoshariati, H.; Pouretedal, H.R.; Tehrani, M.K.; Semnani, A. Prediction of Shock Sensitivity of Explosives Based on Small-Scale Gap Test. *J. Hazard. Mater.* **2007**, *145*(1): 109-112.
[12] Anderson, E. Explosives, Tactical Missile Warheads. *AIAA* **1993**, *155*: 113.
[13] Rezaei, A.H.; Keshavarz, M.H.; Tehrani, M.K.; Darbani, S.M.R.; Farhadian, A.H.; Mousavi, S.J.; Mousaviazar, A. Approach for Determination of Detonation

Performance and Aluminum Percentage of Aluminized-Based Explosives by Laser-Induced Breakdown Spectroscopy. *Appl. Opt.* **2016**, *55*(12): 3233-3240.

[14] Rezaei, A.; Keshavarz, M.; Tehrani, M.K.; Darbani, S. Quantitative Analysis for the Determination of Aluminum Percentage and Detonation Performance of Aluminized Plastic Bonded Explosives by Laser-Induced Breakdown Spectroscopy. *Laser Phys.* **2018**, *28*(6): 065605.

[15] Makhov, M.; Gogulya, M.; Dolgoborodov, A.Y.; Brazhnikov, M.; Arkhipov, V.; Pepekin, V. Acceleration Ability and Heat of Explosive Decomposition of Aluminized Explosives. *Combust. Explos. Shock Waves* **2004**, *40*(4): 458-466.

[16] Trzciński, W. Application of a Cylinder Test for Determining Energetic Characteristics of Explosives. *J. Tech. Phys.* **2001**, *42*(2): 165-179.

[17] Zhou, Z.; Nie, J.; Ou, Z.; Qin, J.; Jiao, Q. Effects of the Aluminum Content on the Shock Wave Pressure and the Acceleration Ability of RDX-Based Aluminized Explosives. *J. Appl. Phys.* **2014**, *116*(14): 144906.

[18] Vadhe, P.; Pawar, R.; Sinha, R.; Asthana, S.; Rao, A.S. Cast Aluminized Explosives. *Combust. Explos. Shock Waves* **2008**, *44*(4): 461-477.

[19] Zhang, F.; Anderson, J.; Yoshinaka, A. Post-Detonation Energy Release from TNT-Aluminum Explosives. *AIP Conference Proceedings,* AIP, **2007**, 885-888.

[20] Lu, J.P.; Dorsett, H.E.; Franson, M.D.; Cliff, M.D. *Near-field Performance Evaluations of Alex Effect in Metallised Explosives.* DSTO Report, **2003**.

[21] Swisdak, (Jr) M.M. *Explosion Effects and Properties. Part II. Explosion Effects in Water.* NSWC Report, **1978**.

[22] Stromsoe, E.; Eriksen, S. Performance of High Explosives in Underwater Applications. Part 2: Aluminized Explosives. *Propellants Explos. Pyrotech.* **1990**, *15*(2): 52-53.

[23] Xiang, D.L.; Rong, J.L.; Li, J. Effect of Al/O Ratio on the Detonation Performance and Underwater Explosion of HMX-based Aluminized Explosives. *Propellants Explos. Pyrotech.* **2014**, *39*(1): 65-73.

[24] Keicher, T.; Happ, A.; Kretschmer, A.; Sirringhaus, U.; Wild, R. Influence of Aluminium/Ammonium Perchlorate on the Performance of Underwater Explosives. *Propellants Explos. Pyrotech.* **1999**, *24*(3): 140-143.

[25] Masahiko, N.; Aoki, A.; Miyoshi, H. Effects of Aluminum on the Energy of Underwater Explosion for the Insensitive PBXs. *Insensitive Munitions of Technology Symposium* **1997**, 19-21.

[26] Brousseau, P.; Anderson, C.J. Nanometric Aluminum in Explosives. *Propellants Explos. Pyrotech.* **2002**, *27*(5): 300-306.

[27] Farhadian, A.H.; Tehrani, M.K.; Keshavarz, M.H.; Darbani, S.M.R. Energetic Materials Identification by Laser-Induced Breakdown Spectroscopy Combined with Artificial Neural Network. *Appl. Opt.* **2017**, *56*(12): 3372-3377.

[28] Farhadian, A.H.; Tehrani, M.K.l Keshavarz, M.H.; Karimi, M.; Darbani, S.M.R. Relationship Between the Results of Laser-Induced Breakdown Spectroscopy and Dynamical Mechanical Analysis in Composite Solid Propellants During their Aging. *Appl. Opt.* **2016**, *55*(16): 4362-4369.

[29] Farhadian, A.H.; Tehrani, M.K.; Keshavarz, M.H.; Karimi, M.; Darbani, S.M.R.; Rezayi, A.H. A Novel Approach for Investigation of Chemical Aging in Composite Propellants Through Laser-Induced Breakdown Spectroscopy (LIBS). *J. Therm. Anal. Calorim.* **2016**, *124*(1): 279-286.
[30] Gottfried, J.L.; De Lucia, F.C.; Munson, C.A.; Miziolek, A.W. Laser-Induced Breakdown Spectroscopy for Detection of Explosives Residues: A Review of Recent Advances, Challenges, and Future Prospects. *Anal. Bioanal. Chem.* **2009**, *395*(2): 283-300.
[31] Parigger, C.G. Atomic and Molecular Emissions in Laser-Induced Breakdown Spectroscopy. *Spectrochim. Acta, Part B: Atomic Spectroscopy* **2013**, *79*: 4-16.
[32] Fernández-Bravo, Á.; Delgado, T.; Lucena, P.; Laserna, J.J. Vibrational Emission Analysis of the CN Molecules in Laser-Induced Breakdown Spectroscopy of Organic Compounds. *Spectrochim. Acta, Part B: Atomic Spectroscopy* **2013**, *89*: 77-83.
[33] Gottfried, J.L. Laser-Induced Plasma Chemistry of the Explosive RDX with Various Metallic Nanoparticles. *Appl. Opt.* **2012**, *51*(7): B13-B21.
[34] Lucena, P.; Doña, A.; Tobaria, L.; Laserna, J. New Challenges and Insights in the Detection and Spectral Identification of Organic Explosives by Laser Induced Breakdown Spectroscopy. *Spectrochim. Acta, Part B: Atomic Spectroscopy* **2011**, *66*(1): 12-20.
[35] Lazic, V.; Palucci, A.; Jovicevic, S.; Poggi, C.; Buono, E. Analysis of Explosive and Other Organic Residues by Laser Induced Breakdown Spectroscopy. *Spectrochim. Acta, Part B: Atomic Spectroscopy* **2009**, *64*(10): 1028-1039.
[36] Lasheras, R.; Bello-Galvez, C.; Rodriguez-Celis, E.; Anzano, J. Discrimination of Organic Solid Materials by LIBS Using Methods of Correlation and Normalized Coordinates. *J. Hazard. Mater.* **2011**, *192*(2): 704-713.
[37] Fink, H.; Panne, U.; Niessner, R. Process Analysis of Recycled Thermoplasts from Consumer Electronics by Laser-Induced Plasma Spectroscopy. *Anal. Chem.* **2002**, *74*(17): 4334-4342.
[38] Martin, M.Z.; Labbé, N.; Rials, T.G.; Wullschleger, S.D. Analysis of Preservative-Treated Wood by Multivariate Analysis of Laser-Induced Breakdown Spectroscopy Spectra. *Spectrochim. Acta, Part B: Atomic Spectroscopy* **2005**, *60*(7): 1179-1185.
[39] Alamelu, D.; Sarkar, A.; Aggarwal, S. Laser-Induced Breakdown Spectroscopy for Simultaneous Determination of Sm, Eu and Gd in Aqueous Solution. *Talanta* **2008**, *77*(1): 256-261.
[40] Pandhija, S.; Rai, N.; Rai, A.K.; Thakur, S.N. Contaminant Concentration in Environmental Samples Using LIBS and CF-LIBS. *Appl. Phys. B* **2010**, *98*(1): 231-241.
[41] Rai, N.K.; Rai, A.K.; Kumar, A.; Thakur, S.N. Detection Sensitivity of Laser-Induced Breakdown Spectroscopy for Cr II in Liquid Samples. *Appl. Opt.* **2008**, *47*(31): G105-G111.
[42] Keshavarz, M.H. New Method for Predicting Detonation Velocities of Aluminized Explosives. *Combust. Flame* **2005**, *142*(3): 303-307.

[43] Keshavarz, M.H. Predicting Maximum Attainable Detonation Velocity of CHNOF and Aluminized Explosives. *Propellants Explos. Pyrotech.* **2012**, *37*(4): 489-497.
[44] Keshavarz, M.H. Prediction of Detonation Performance of CHNO and CHNOAL Explosives Through Molecular Structure. *J. Hazard. Mater.* **2009**, *166*(2-3): 1296-1301.
[45] Keshavarz, M.H. Simple Correlation for Predicting Detonation Velocity of Ideal and Non-Ideal Explosives. *J. Hazard. Mater.* **2009**, *166*(2-3): 762-769.
[46] Ralchenko, Y.; Kramida, A.; Reader, J.; Team, N. NIST Atomic Spectra Database (version 4.0). National Institute of Standards and Technology, Gaithersburg, MD, **2010**.
[47] Ma, Q.; Dagdigian, P.J. Kinetic Model of Atomic and Molecular Emissions in Laser-Induced Breakdown Spectroscopy of Organic Compounds. *Anal. Bioanal. Chem.* **2011**, *400*(10): 3193-3205.
[48] Mousavi, S.; Farsani, M.H.; Darbani, S.; Mousaviazar, A.; Soltanolkotabi, M.; Majd, A.E. CN and C_2 Vibrational Spectra Analysis in Molecular LIBS of Organic Materials. *Appl. Phys. B* **2016**, *122*(5): 106.
[49] Dong, M.; Lu, J.; Yao, S.; Zhong, Z.; Li, J.; Li, J.; Lu, W. Experimental Study on the Characteristics of Molecular Emission Spectroscopy for the Analysis of Solid Materials Containing C and N. *Opt. Express* **2011**, *19*(18): 17021-17029.
[50] Lasheras, R.; Bello-Gálvez, C.; Anzano, J. Quantitative Analysis of Oxide Materials by Laser-Induced Breakdown Spectroscopy with Argon as an Internal Standard. *Spectrochim. Acta, Part B: Atomic Spectroscopy* **2013**, *82*: 65-70.
[51] Keshavarz, M.H.; Zamani, A.; Shafiee, M. Predicting Detonation Performance of CHNOFCl and Aluminized Explosives. *Propellants Explos. Pyrotech.* **2014**, *39*(5): 749-754.
[52] Keshavarz, M.H.; Mofrad, R.T.; Poor, K.E.; Shokrollahi, A.; Zali, A.; Yousefi, M.H. Determination of Performance of Non-Ideal Aluminized Explosives. *J. Hazard. Mater.* **2006**, *137*(1): 83-87.
[53] Zhou, Z.Q.; Nie, J.X.; Zeng, L.; Jin, Z.X.; Jiao, Q.J. Effects of Aluminum Content on TNT Detonation and Aluminum Combustion Using Electrical Conductivity Measurements. *Propellants Explos. Pyrotech.* **2016**, *41*(1): 84-91.
[54] Keshavarz, M.H.; Zamani, A. A Simple and Reliable Method for Predicting the Detonation Velocity of CHNOFCl and Aluminized Explosives. *Cent. Eur. J. Energ. Mater.* **2015**, *12*(1): 13-33.
[55] Parigger, C.G.; Woods, A.C.; Surmick, D.M.; Gautam, G.; Witte, M.J.; Hornkohl, J.O. Computation of Diatomic Molecular Spectra for Selected Transitions of Aluminum Monoxide, Cyanide, Diatomic Carbon, and Titanium Monoxide. *Spectrochim. Acta, Part B: Atomic Spectroscopy* **2015**, *107*: 132-138.
[56] Witte, M.; Parigger, C. Laser-Induced Spectroscopy of Graphene Ablation in Air. *J. Phys.: Conf. Ser. 548* **2014**, IOP Publishing 012052.

Received: June 5, 2018
Revised: November 25, 2018
First published online: March 5, 2019